Chasm: A Screw Based Expressive Compact Haptic Actuator

Pornthep Preechayasomboon
University of Washington
Seattle, WA, USA
prnthp@uw.edu

Ali Israr
Facebook Reality Labs
Redmond, WA, USA
aliisrar@fb.com

Majed Samad
Facebook Reality Labs
Redmond, WA, USA
majedsamad@fb.com

Figure 1. (left) A render of Chasm with a reference scale, the red arrow and wave represents how Chasm can simultaneously render both shear/normal forces and vibrations, (middle) A headgear prototype with two Chasm units on adjacent sides of the temple area on the head for enhancing locomotion in virtual reality (VR). A representative VR headset is shown. (right) A marker prototype with an embedded Chasm unit for enhancing interaction in augmented reality (AR) and virtual reality (VR), the hand is tracked with an attached Oculus Touch controller. The outlines show where Chasm is embedded in the prototypes.

ABSTRACT

We present a compact broadband linear actuator, *Chasm*, that renders expressive haptic feedback on wearable and handheld devices. Unlike typical motor-based haptic devices with integrated gearheads, Chasm utilizes a miniature leadscrew coupled to a motor shaft, thereby directly translating the high-speed rotation of the motor to the linear motion of a nut carriage without an additional transmission. Due to this simplicity, Chasm can render low-frequency skin-stretch and high-frequency vibrations, simultaneously and independently. We present the design of the actuator assembly and validate its electromechanical and perceptual performance. We then explore use cases and show design solutions for embedding Chasm in device prototypes. Finally, we report investigations with Chasm in two VR embodiments, i.e., in a headgear band to induce locomotion cues and in a handheld pointer to enhance dynamic manual interactions. Our explorations show wide use for Chasm in enhancing user interactions and experience in virtual and augmented settings.

Author Keywords

Skin stretch; multidimensional haptics; haptic devices; handheld haptics; wearable haptics.

Permission to make digital or hard copies of all or part of this work for personal or classroom use is granted without fee provided that copies are not made or distributed for profit or commercial advantage and that copies bear this notice and the full citation on the first page. Copyrights for components of this work owned by others than the author(s) must be honored. Abstracting with credit is permitted. To copy otherwise, or republish, to post on servers or to redistribute to lists, requires prior specific permission and/or a fee. Request permissions from permissions@acm.org.
CHI 2020, April 25–30, 2020, Honolulu, HI, USA.
© 2020 Copyright is held by the owner/author(s). Publication rights licensed to ACM. ACM ISBN 978-1-4503-6708-0/20/04...$15.00.
DOI: https://doi.org/10.1145/3313831.3376512

CCS Concepts

• **Human-centered computing~Human computer interaction (HCI)**; *Haptic devices*; User studies;

INTRODUCTION

Human touch is critical for users' engagement with the surrounding environment and enables physical interactions with objects around them. Users reach out to pick objects, move them around and perform tasks while tuning their motor commands in response to dynamic interactions between the users' touch system and the objects' behavior. Despite this rich information flow between physical objects and the human touch system, current solutions to enable artificial touch feedback (or haptic feedback) are limited. Most commonly, vibrotactile actuators are incorporated in handheld devices and controllers to provide feedback of tactile contacts, impacts, button clicks, and surface texture [5,12,26]. The popularity of these actuators is due to their compact and lightweight design and low power requirements.

On the other end of the spectrum, low-frequency haptic devices that indent or stretch the skin can render percepts of dynamic behaviors of virtual objects comparable to the inertia and stiffness of objects [9,19,29]. The embedded actuators in these prototypes, however, have low bandwidth, are larger in size, have complex transmissions with non-linear system dynamics, and have relatively high-power requirements. Researchers have also accommodated both low-frequency dynamic effects and high-frequency vibrations in a single device by utilizing separate low- and high-frequency actuators to broaden the capacity and fidelity of haptic feedback [2,4,7,14,23]. However, similar to the

low-frequency actuators, these multi-dimensional actuators are bulky, and not practical for handheld and wearable applications.

In this paper, we introduce *Chasm*: a Compact Haptic Actuator with a Screw Mechanism. Chasm utilizes a common mechanical element, the leadscrew, which is found in many consumer grade devices. By coupling a leadscrew directly to a miniature high-speed DC motor, Chasm can render constant skin-shear as well as high-frequency vibrations both independently and simultaneously, therefore enabling high definition haptic feedback using a small actuator assembly. We present the design of Chasm and explore its use cases in a variety of wearable and handheld embodiments. We optimize the design of a leadscrew mechanism and embed it in (i) a head mounted system to induce navigational and locomotion cues and (ii) a handheld pointer to interact with broadband dynamic behaviors of virtual objects (Figure 1). In a series of engineering and user testing, we demonstrate high bandwidth and high fidelity of our design and its capacity to augment user interactions and experiences.

We present the following contributions:

(1) We present the design and implementation of a compact screw-based one-degree-of-freedom haptic actuator capable of rendering broadband and high-fidelity haptic effects., e.g. low frequency skin-shear combined with high-frequency vibrations or independently.
(2) We validate the actuator design with engineering and perceptual tests
(3) We explore an interaction space and potential form factors using our device
(4) We investigate two exemplary use cases and corresponding psychophysical evaluations to highlight their utility

BACKGROUND

Mechanical stimulations on the body are felt through cutaneous (or tactile) and kinesthetic systems. *Cutaneous* receptors are embedded in the dermis and epidermis of the skin, and are activated by skin deformation due to indentation, stretch, texture, friction, and vibration [16]. These receptors are sensitive to near DC to ~500 Hz and peak at around 250 Hz [3], and can be activated by minuscule displacements and forces which saturate at a few millimeters of displacement and few Newtons of force [13]. *Kinesthetic* receptors are located in joints, muscles and tendons and detect joint movements and muscular activities. These receptors have small bandwidth (<20Hz) and operate in higher force and displacement ranges [18].

Common haptic actuators used in consumer devices are typically based on voice coil technology, such as the linear resonator actuator or LRA [5] and the eccentric rotating mass or ERM. Both actuators are small in size, have few components, and consume low power to create a noticeable haptic effect. They are used in game controllers, mobile devices, watches, and many other wearable and handheld devices. These actuators are designed to operate in the high-frequency vibration range (>100 Hz), where the sensitivity of human perception is high and low displacements are sufficient to create percepts [3]. Driving these actuators at lower frequencies, however, may compromise with the overall efficiency such as size, weight, power consumption and heat dissipation. Piezoceramic based actuators are also available in compact formfactors, but they are also limited by high-frequency and low-displacement applications [26].

For low-frequency haptic feedback, recent research has utilized typical motors with custom transmission for skin stretch and skin indentation applications. Gear-trains or harmonic-drives first step-down the high motor speed and a custom mechanism converts the rotating shaft to linear motion. Prototypes have been built with pulley-cable [23,27], belt [20], roller-gear [37], scotch-yoke [17], delta mechanism [33], and gear-rocker [7] drives and then embedded in wearable and handheld devices. These devices can render high fidelity dynamics of virtual objects and produce sensations of movement, stiffness, inertia and squeeze [10,23,33]. Their use is however limited due to the relatively high number of components for transmission and therefore have higher cost, low reliability, audible noise between mechanical components, low output bandwidth, variability in performance in the operating range, and limited scalability to various formfactors.

Another compact haptic actuator is the Foldaway linkage by Salerno and colleagues [21], which uses an origami structure and micromotors to move a compact foldable platform against finger movements, hereby modulating the stiffness of virtual objects in contact up to 2 N. Recent research has also explored soft actuators, such as pneumatic and electroactive polymers for their compact and flexible housings, however, their use for wearable and handheld devices are limited due to oversized pressure sources (such as a compressor cylinder) or high driving voltages (beyond normal safety ranges). However, these actuators show potential for future use in wearable and handheld technologies [38,39].

A common rendering haptic primitive is *skin stretch*, which has been used to display friction [30] and inducing directional cues for driving guidance [25]. Skin stretch has also been used to display forces tangentially to finger pads, to simulate gravity [19] or other forces [22,36]. Tactors are placed in a pen type end effector to give force feedback and guidance cues [31], in a handheld device to create forces and torques [30], or mounted directly to the fingertip to render both contact force and weight [33]. In addition to the fingertip feedback, skin stretch can display information to the arms and other body locations [11,14]. Recent research has also explored multidimensional haptic cues and sensory illusions in rich sensory environments and provided users with believable and expressive feedback [4,7,14]. Several researchers have also employed none to low-quality haptic feedback with altered visual interactions and showed

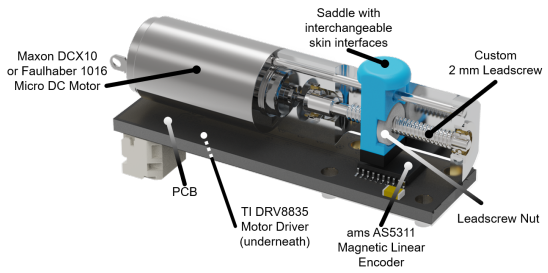

Figure 2. A cutaway section showing the mechanical and electrical components of Chasm

enhanced perception of weight and other dynamic forces in virtual environments [15,32]. Based on these studies, it is hypothesized that low profile skin deformations can substantially improve user interactions with objects in dynamic virtual environment, without the need of high force kinesthetic cues for a believable sensory experience.

Recently, Sreetharan and colleagues investigated lead screw drives to directly convert the high rotational speed of a *stepper* motor to linear motion without the need of an intermediate transmission mechanism [34]. Their prototype was compact (8 mm × 13 mm × 27 mm; 5 grams) and had high output performance (max. force: ~1 N, 5 mm stroke at ~100 mm/s with 2 W of maximum power consumption). However, the performance of the actuator was substantially depreciated when a finger was loaded on the moving saddle, reducing both the stroke of the saddle and its bandwidth due to the open loop control scheme to command the motor [34]. In this paper, we optimize the design of a screw directly-driven by a DC motor, specifically without the use of intermediate gearheads or step-down mechanisms, using a PI (proportional-integral) feedback control law to maintain high bandwidth and reduced finger loading effects, and explore its usability in a variety of wearable and handheld configurations.

DESIGN

Chasm's core design element is a motor coupled directly to a leadscrew, that is, without any additional transmission or step-down mechanisms between the motor and the leadscrew. Chasm was also designed to have a minimal number of components: a DC motor without an integrated gearhead, a custom leadscrew and nut, two bearings, and a housing. Our design process began by evaluating numerous leadscrew and motor manufacturers. Although some motor manufacturers offer motors with leadscrew shafts, these motors are often stepper motors which could not perform within our performance envelope [34]. Brushless direct current (BLDC) motors were also considered, but ultimately brushed direct current (DC) motors were chosen due to their simplicity to control and compact size. The leadscrew manufacturer, Ametek, was chosen mainly due to their capability in producing custom high-precision, low-friction leadscrews and leadscrew nuts. Through a process of evaluation of various combinations of leadscrews and motors, we finalized on pairing the 12 Volt Faulhaber 1016 [40] DC motor with a customized LSS series 2 mm leadscrew with a 1 mm lead [41], due to the satisfactory linear speed at nominal motor speed and excess in force output to accommodate for any frictional losses. With modularity in mind, the leadscrew nut has a simple flanged design with flats to accommodate 3D printed extensions. Figure 2 shows a sectional model of Chasm with the internal components visible.

In order to track the position of the leadscrew, Chasm was designed to have a magnetic encoder placed directly underneath the leadscrew assembly. The Austria Microsystems (ams) AS5311 [42] was chosen due to its high bandwidth, high resolution and ease of integration. A magnetic strip with alternating poles every 1 mm serves as the tracker, which is bonded directly to the leadscrew nut. The Texas Instruments (TI) DRV8835 [43] was chosen to drive the motors due its compact size, low operating voltage and high current capability. Furthermore, with compactness and efficiency in mind, both the magnetic encoder and motor driver are assembled on to the same printed circuit board (PCB) that is mounted underneath the leadscrew and motor.

Lastly, a custom machined housing, two micro bearings and a 1 mm diameter shaft serve as the main structural elements. The bearings that are press-fit into the housing provide rigidity and constraints for normal and thrust loads for the leadscrew. The 1 mm diameter shaft constrains the nut from rotating while minimizing sliding friction. The overall size of Chasm excluding the wiring terminal is approximately 11 mm × 14 mm × 45 mm.

Closed-loop Control Law

Chasm achieves closed loop control by reading the ams AS5311 magnetic encoder as input for the position of the leadscrew nut and sending correction commands to the TI DRV8835 motor driver. A PJRC Teensy 3.5 ARM Cortex-M4 microcontroller was used to maintain an interrupt-driven 1000 Hz proportional-integral (PI) controller on up to two Chasm units. The gains of the controller are selected to achieve a high gain crossover frequency for faster response time and a low overshoot, compensating for skin-loading disturbances and reducing structural and resonant harmonics in the DC to 100 Hz range.

Information Flow Framework

As Chasm is designed to be prototyped in various use cases, a robust software framework that can adapt to various scenarios is required. Firstly, in order to reduce guesswork in latency of haptic rendering, we used the universal serial bus human interface device (USB HID) class for communicating between the rendering device and the Teensy microcontroller in "Raw HID" mode. USB HID has two major benefits: (i) it has plug and play capability for most devices on the market, including consumer VR devices such as the Oculus Quest, most Android smartphones and most modern PCs running Windows, Linux or macOS, which eliminates the need for custom drivers, (ii) USB HID requires the host device to reserve bandwidth for HID, which is only 64 bytes per

millisecond, however, if a command packet is less than 64 bytes, the latency is ideally 1 millisecond.

Then, to increase scalability and aid development time, protocol buffers (protobuf) is used as a serialization layer, i.e. structured data is translated to protobuf binary data before sending or receiving the data between devices [44]. Consequently, typical packets being sent to the microcontroller, such as commands to move the end effector (leadscrew nut) to a specific position, are 6-10 bytes in size, which is well below the 64 bytes bandwidth for 1 ms latency. Another benefit is protobuf supports most popular programming languages, including C# and C++. We use the protobuf-unity [24] library for our Unity (C#) implementation and nanopb [1] for our microcontroller (C++) implementation.

Our implementation of the framework is as follows. On the firmware side, the microcontroller, while running the PI control loop, concurrently waits for a packet coming in from USB HID. The packet contains information such as the desired position for each Chasm unit, the speed in which to translate to that position, a command to play back stored sequences of positions or the sequences themselves (uploading waveforms). Once a packet is received and deserialized, the microcontroller immediately updates all state variables for the motors or performs the commanded actions. The microcontroller can also send data back to the host device using the same protocol for diagnostics. Figure 3 shows an overview of the framework.

Finally, we created operating system (OS) specific linked libraries (also known as plug-ins) for Windows, macOS, and Android. These plugs-ins can then be integrated into most applications that run on the system. In this paper, we exclusively use the Unity game engine with our plug-ins because of its multi-platform and VR capabilities. Unity can then be used as a simulation engine to drive both the visuals and haptics, letting users and the actuator react to both modalities seamlessly.

DESIGN VALIDATION

With the proper control architecture in place, we can command the actuator to move the end effector with various displacement profiles under different loading conditions. To verify that Chasm, once integrated, can render various haptic effects from constant skin-stretch to high frequency vibrations, the following section presents results from experiments for validating the actuator's performance. We also summarize the comparison of Chasm's performance to other research prototypes in Table 1.

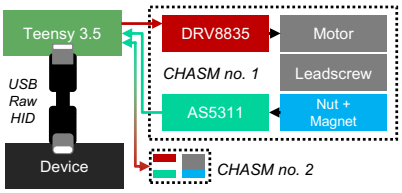

Figure 3. The overall architecture for Chasm's controller.

Device	Vol. (cm^3)	Wt. (g)	Work-space (mm)	Force Max (N)	Freq. Max (Hz)	Freq. -3 dB (Hz)	Power (W)
Chasm	6.54	15	3.4	4.8	170	20	0.6 – 2.7
Sreetharan [34]	1.87	5	6	1.5	15	4	< 2
Tian [35]	121	100	18	3.23	-	-	-
Clemente [6]	52	60	6	8.6	30	5.5	-
hRing [22]	10.4	15	-	0.3	-	-	-
HapTip [8]	24.3	22	4×4	3.4	-	-	-
Schorr [33]	42.0	32	10×10×5	7.5	30	~15	-
Foldaway [21]	188	130	35×35×30	2	140	20	-

Table 1. Comparison between Chasm's performance and similar research devices – unavailable data is represented with a dash

Temporal Response

The magnetic encoder was validated first to determine its usability as a sensor. We fitted a prototype of Chasm with a nut extension with a reflective marker, as shown in Figure 4a, and used a laser doppler vibrometer (Polytec PSV-500) to measure the actual displacement compared to the encoder readout. Figure 4b and Figure 4c show that the encoder has a linear response and can be trusted to provide accurate position tracking down to 100 microns. All subsequent experiments were performed using the magnetic encoder exclusively as positional tracking ground truth.

Unloaded Step Response. We ran a series of step response tests, in both the unloaded and loaded conditions. The actuator has an average rise time of 12.9 milliseconds and a steady-state error of 40 microns, as reported by the encoder and shown in Figure 4f. The top, no-load, speed of the actuator, as calculated from the rise time, is 217 mm/second.

Loaded Step Response. To put the actuator under nominal loading conditions, we first constructed mock prototypes with embedded capacitive force sensors to determine the usual normal loading. These mock prototypes reflect the use-cases in later sections and all loading conditions tested here are extreme loadings on the mock prototypes.

The loaded step response in Figure 4g shows that the actuator can still render displacement under a normal loading of 3.6 N with a constant displacement error of 150 microns.

Blocked Force Response. We also ran a blocked force response test, with the setup shown in Figure 4d. The results, Figure 4e, show that the actuator can reach the steady state force of 4.8 N. The response characteristics can be further improved by tuning the derivative part of the PID control law. However, the design of a new and accurate control law is beyond the scope of this paper.

Frequency Response

To validate the extent of Chasm's bandwidth, we ran a series of frequency response experiments.

Chirp Response. Chasm was commanded a sinusoidal waveform that swept from 0.5 to 40 Hz at a constant

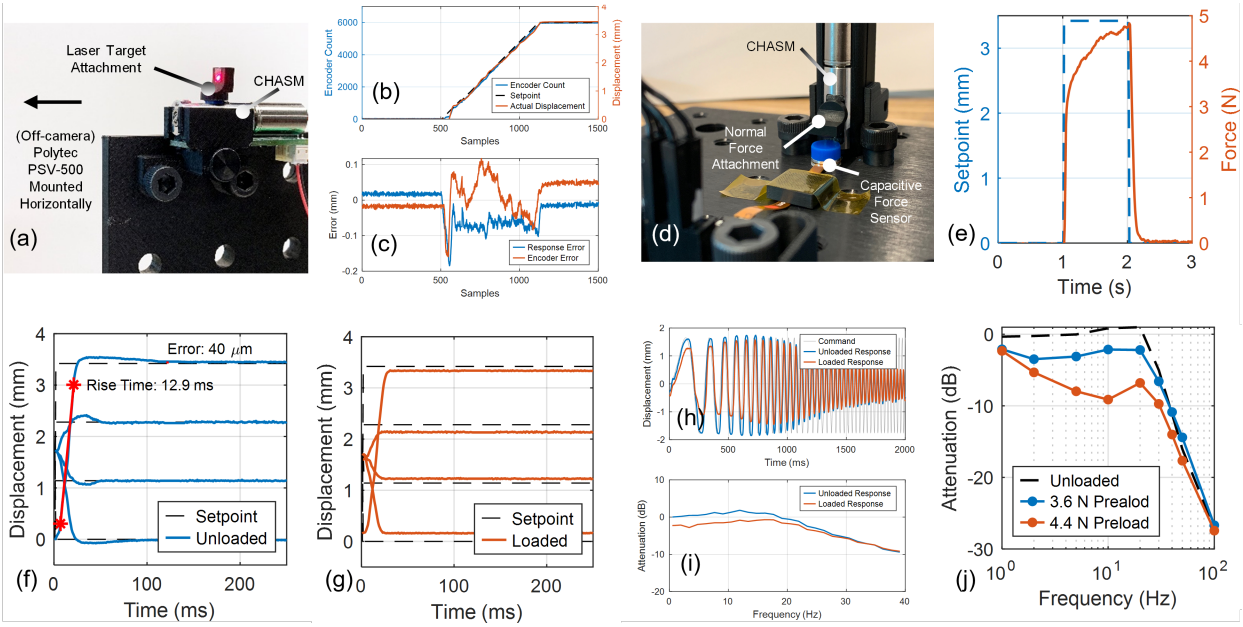

Figure 4. (a) The experimental setup for validating Chasm's encoder output (b) & (c) Plots showing the tracking error between Chasm's encoder and the laser vibrometer readings (d) The experimental setup for measuring Chasm's force output. (e) A plot showing the blocked force response given a step input of 3.4 mm (f) A plot showing the overall rise time of 12.9 ms, given an unloaded step input and the steady-state error of 40 microns (g) A plot showing the loaded step response with a 3.6 N preload (h) & (i) Plots showing the unloaded and loaded frequency response of a chirp signal from 0.5 to 40 Hz (j) A plot comparing the attenuation between the unloaded and loaded frequency response of 3.6 N and 4.4 N of preload at various frequencies up to 100 Hz

amplitude of 1.71 mm (3.42 mm peak-to-peak) for a duration of 2 seconds. Figure 4h shows temporal response of Chasm's carriage displacement, and Figure 4i shows the frequency response with gain-crossover frequency around 20 Hz.

Sinusoidal Response. In a separate experiment, Chasm was commanded with sinusoidal frequencies from 1 Hz up to 100 Hz at amplitudes from 0.15 to 1.71 mm. The results shown in Figure 4j represent the mean attenuation across all amplitudes and loading conditions. The frequency response shows that Chasm has a significant attenuation above 20 Hz.

Human Perception Bandwidth

Although the results in the frequency response characterization show that the actuator's output is significantly attenuated at frequencies higher than 20 Hz, we ran a pilot study to show that rendered frequencies above 20 Hz can still be perceived, up to 170 Hz, as in Figure 5.

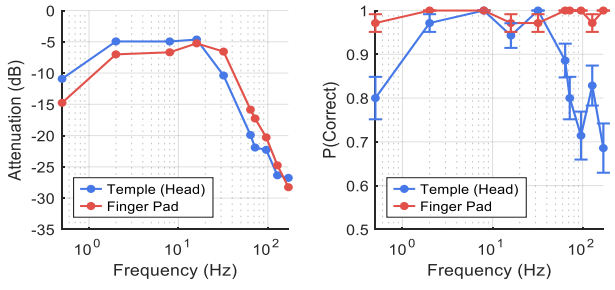

Figure 5. (left) A plot of the average attenuation when loaded on the head and finger at various frequencies. (right) The average responses of identifying the correct interval for each condition

Seven participants, (7 males, aged 26 to 44) held a handheld prototype with their thumb resting on the actuator's end effector for measuring the finger's perceivability and a headgear prototype with the actuator touching the right side of the temple (as shown in Figure 1). Participants experienced two intervals of stimuli, either the first or second interval had the actuator active and participants would answer in which interval they felt the stimulus. The stimulus were displacements in a sine wave from 0.5 Hz to 170 Hz at a constant amplitude of 0.428 mm for 1 second. Participants also wore noise cancelling headphones with a tone played in the same frequency as the actuator at each interval to mask out any audible cues.

The results are shown in Figure 5 for the finger pad (red) and temple (blue). Even though the actuator's response is dampened significantly, it is still perceivable from 0.5 Hz to 170 Hz on the hand and from 0.5 to 72 Hz on the head. Beyond 128 Hz, participants reported that the whole device vibrated and was perceivable by the hand. This could be due to aliasing and the limited sample rate of our controller which is currently set to 1000 Hz.

Power Consumption

During the blocked force response experiment, we captured a peak current consumption of 225 mA at 12 Volts. Assuming a 60% output loss due to mechanical and electrical efficiencies, we can approximate the power density of Chasm to be 166 kW/m^3. However, during normal operation, such as rendering a 100 Hz sine wave at 0.25 mm amplitude or moving the end effector from resting to 2 mm, we observe

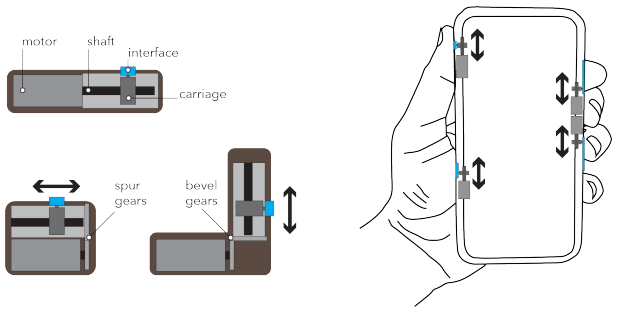

Figure 6. (left) Design variation of the screw mechanism. Direct drive lead screw (top) and folded and beveled designs (bottom) of the screw mechanism. (right) multiple screw mechanism are used in a cell phone case to distribute multi-finger interactions.

only peak momentary current consumption from 50 to 120 mA. Furthermore, for certain conditions such as rendering a constant force, since Chasm's leadscrew is self-locking and non-backdrivable, we can simply drive Chasm to its intended position and cease to supply power since the position will be held regardless of power input.

USE CASE EXPLORATIONS

Chasm presents many advantages for haptic devices and is highly scalable. In this section, we highlight these advantages in a variety of embodiments and explore its design and interaction spaces. The benefits of Chasm are its broad bandwidth and flexible design configurations that enables the realization of high-fidelity haptic interactions embedded in a variety of wearable and handheld devices.

Wide Bandwidth and Linearity

Chasm has broad bandwidth compared to previously reported devices. We achieved this performance by using small and fewer components and optimize the actuator response by using a PI feedback control law that achieves high response time, operating range linearity, disturbance rejection, and near DC to >100 Hz perceivable frequency range. Many previous voice-coil solutions operate in broad frequency response from ~30-500 Hz, which covers most of the vibrotactile range of human perception, however driving them at low-frequency movement profiles increase the size, power and heat generation. Due to low back drivability and the operating nature of the screw mechanism, Chasm's response is highly linear and consistent in its operating range; and can render both low-frequency (or low velocity) force-displacement profiles as well as high-frequency vibrotactile sensations, therefore extends into the broader dynamic range of human haptic perception.

Flexible Design Solutions

Compact, restricted and complex spaces

Chasm is housed in compact and small casing and can be directly integrated in hardware prototypes. For smaller profiles, a smaller size motor can be utilized, such as [34] achieved ~1 N of force with a 5-gram design. In more restricted and complex spaces, screw mechanisms can be folded and/or beveled by using a pair of spur or bevel gears, as shown in Figure 6a. These gears have high efficiencies (up to 95%) due to small step-down speed and produce low

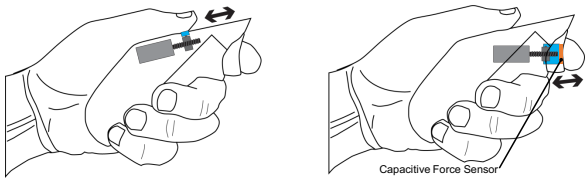

Figure 7. A hand controller embedded with Chasm in (a) shear mode and (b) normal mode, with an inline capacitive force sensor to help emulate back-drivability

noise, and therefore compromises in the design extends the usability into many formfactors. Multiple Chasm units can be embedded in a device to distribute the load and interactions through independent contact locations with the device (Figure 6b), and screw linkages can also be a part of the overall structure of the device and provides resisting forces against user's loading.

Multidimensional Configurations

In the design shown in the previous section, the rotational motor shape is translated to the linear carriage motion that is coupled to the skin interface. A typical application is sliding against the skin to shear or stretch the skin. A different coupling adapter can be used to translate the carriage motion to indent into the skin. Figure 7a shows a hand controller embedded with Chasm in shear mode to stretch the skin of the thumb, and Figure 7b shows Chasm in a normal force configuration to resist against the finger motion in a trigger-like action, where back drivability is emulated using an inline force sensor.

Formfactors and User Experiences

Typical applications of Chasm are in *handheld* devices, where the linear motion of Chasm is interfaced with the skin of the fingers and palm and enhances dynamic interactions during manual tasks. It can be placed in a compact **game controller** or in the casing of a **cellphone** to render directional cues for navigations, surface texture during object explorations, stiffness and weight cues for object manipulation, dynamic shaking during collisions, and enhanced feedback with user interface widgets, such as in a button press or a slider motion. Another use case is a **stylus** shaped marker used as a writing device on flat surfaces and the embedded Chasm stretches the finger skin to render virtual textures and topology on the surface and alter mechanical features of virtual objects, as shown in Figure 8. Similar interactions can be done in mid-air with a pointing device, where the skin stretch of the finger enhances user interactions with pull-push like sensations and allow users to perform dynamic manual tasks, such as feeling compliance and weight of virtual objects – for example see [35].

Another utility of Chasm is in *wearable* devices, where the compact actuator stretches the skin to induce locomotion cues. In **shoes**, the actuator stretches the skin of the sole to indicate forward and backward motion while the user slides on virtual ice. A pair of Chasm in a **headband** stretches the skin of the temple on the forehead, and the coordinated motion of each actuator on two sides of the head induces

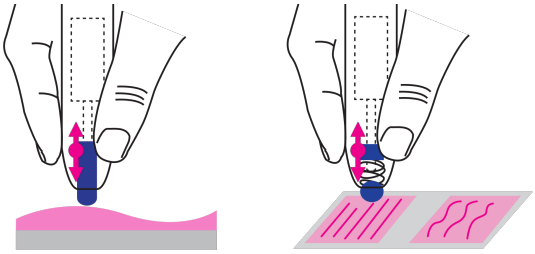

Figure 8. Other stylus-based use cases for a leadscrew-driven design. (left) Driving the height of a stylus tip. (right) Regulating the friction of a ball-point style tip via a spring.

illusion of translational and rotational motion of the head (Figure 9). The backward stretch of temple skin induces forward motion and the forward stretch induces backward motion. In addition to providing directional locomotion cues, stretch cues on the peripheral forehead could modulate motion sickness by inducing corresponding and reactive tactile cues to compensate for the high-speed optic flow through the visual sense.

INTEGRATION AND APPLICATIONS

In this section we discuss about the software architecture to quickly prototype experiences using Chasm and realize common wearable and handheld prototypes. We investigate the use of our actuator (i) in a head-mounted band to render haptic feedback at two sides of the temple to induce locomotion to users, and (ii) in a handheld pointing device to enhance interaction fidelity between the user and virtual objects, and explore use cases in these two settings with a series of user studies. We investigated if the inclusion of haptic cues improves user fidelity and performance bandwidth in rich virtual environments in a set of psychophysical studies presented in this section. All user studies are conducted after ethical and safety reviews by our institution.

Software Workflow for Interactive Gameplay

The Unity game engine, along with the USB HID plug-ins mentioned in the Information Flow Framework section, was used to create experiences for the Oculus Quest. On the development side, we created numerous tools to be used within the Unity Editor to author waveforms and commands that could be instantly tested on Chasm and later preloaded for rapid playback when needed. During real-time simulations, e.g. physics simulations, smaller commands such as "move the end effector to 0.5 mm at 0.5 mm/s" are sent to the controller, enabling responsive interaction scenarios that are directly coupled to the visuals presented. These commands and waveforms are encapsulated in our custom *HapticWaveform* protobuf message that contain data ready to be serialized and transmitted to Chasm's controller firmware. Once the experiences in Unity are ready to be tested or deployed, a compiled android application is sideloaded onto the Oculus Quest. Chasm's microcontroller, the Teensy 3.5, is then plugged directly into the USB Type C receptacle on the Oculus Quest to be used as a standalone device.

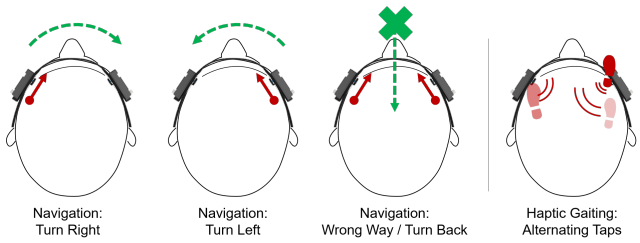

Figure 9. The four different haptic cues rendered by the head mounted device prototype

A Head Mounted Gear to Induce Locomotion

We prototype the headgear by dismantling the head strap from a 3M H-700 series helmet and attaching it to a 3D printed nylon strip with rails on the edges and slots in the middle. We also printed a custom adapter and attached it to Chasm's housing such that the adapter slides on the headband on rails with the moving carriage extending beyond the slot, as shown in Figure 1. We tested several shapes, sizes, texture and material of the interface block, and selected a smooth circular disk (radius 6 mm) made from elastomeric polyurethane (EPU). This disk ensures that Chasm stretches the skin without making the user uncomfortable. We embed a pair of Chasm actuators on two adjacent sides of the headband and adjust the position of the interface to stretch the skin of the temple in the forward and backward direction as shown in Figure 9.

We ran two preliminary studies to investigate the impact of stretch cues on the forehead. Both studies were conducted in a VR environment, where participants wore the headband first to their comfortable levels and then donned an Oculus Quest headset over the band.

In the first study, participants were presented with an optic flow stimulus rendered as a star field moving towards the user and the speed of the optic flow was increased or decreased from a set value during a trial. Each participant's task was to indicate whether the star field motion accelerated or decelerated in the trial. In the visual only (V) condition, the optic flow was rendered at the reference speed of 20 m/s for 1 second followed by 3 seconds of acceleration or deceleration. In the visual-haptics (VH) condition, the visual cue was supplemented with stretch cues either both actuators move backwards (for acceleration) or forwards (for deceleration). Eleven values of change in optic flow speeds were tested (5 accelerated speeds, 5 decelerated speeds and one no change in speed) and the distance of the skin stretch was maintained constant for all VH trials.

Six participants (6 males, ages ranging from 26 to 44, median age: 27 years old) completed two test conditions (V and VH) composed of 88 trials, with 4 repetitions of each level, and the order of the conditions was randomized. Before the experiment, participants were instructed and given a few trials to become familiar with the task and environment.

Figure 10 shows the "proportional of yes" response for participants feeling acceleration (y-axis) as a function of

acceleration of optic flow in the two test conditions. The data is fitted with a psychometric curve using the Palamedes Toolbox [28]. The slope of the psychometric curve near the middle of the plot is steeper in VH condition than the V condition, suggesting better discriminability and multisensory integration in the presence of haptic cues, however, effects of haptic cues were not significant. Using the fitted psychometric curve, we evaluate the just-noticeable-difference (JND) and the point of subjective equality (PSE). Where the JND is 1.728 m/s^2 for the V condition is slightly improved to 1.359 m/s^2 for the VH condition. The PSE point for the V condition is 5.6 m/s^2 and the PSE for the VH condition is 6.114 m/s^2.

In the second study, participants were placed in a VR maze of corridors and the task was to navigate through the maze to find the correct meeting room. An aerial map of the maze was provided to the user with the meeting room marked, however the orientation of the maze and location of the destination room were randomized in each trial, and location of the participant was not indicated on the map. The map is provided in all conditions at the press of a button on the controller.

In no-haptics (No H) conditions, participants navigated through the maze using the map (Figure 11). In haptic-navigation (Nav H) conditions, navigation cues were provided to the participants through the headband. The right actuator stretching forward indicated the participant to turn left and the left actuator stretching forward would indicate a right turn. Both actuators stretching forwards means that the participant is headed the wrong way and should turn back, as shown in Figure 9. Participants were not told about the mapping of haptic feedback and were required to intuitively learn them and use them to complete the task. A third condition, haptic-gaiting (Gait H), was the same as the no-haptics condition except with alternating haptic cues on the two sides of the head corresponding to the gait of users' footsteps during walking, and the tempo of haptics cues was increased during running. The purpose of this condition was to evaluate if the peripheral haptic cues on the forehead have an effect on motion sickness in VR environments.

Ten participants (9 males, ages ranging from 26 to 44, median age: 28 years old) completed the study. Each condition was presented once, and the order of conditions was randomized. Participants were allowed to look at the map as many times as needed and asked to reach the destination as quickly as possible. Participants started with a small corridor where they became familiar with the VR environment and the clock started once they crossed the corridor and entered the maze. Figure 11 shows a birds-eye-view of the map with the proposed directions and the participant's perspective.

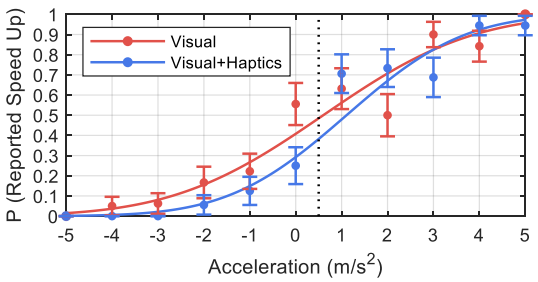

Figure 10. Psychometric plot comparing responses from the V and VH conditions for the acceleration study

Figure 12 shows the overall completion time and subjective evaluation of motion sickness induced due to the VR environment. The haptic-navigation condition yielded lowest completion times ($p<0.01$, paired Student's t-test), while there was no statistical difference between the other two conditions ($p>0.05$). The haptic-gaiting condition also induced lower subjective motion sickness. Participants reported that haptic effects were not annoying, but in fact pleasant and informative, and they were distracted to notice visual motion and were engaged with visual-haptic cues. Participants, however, felt that the head mount gear was tight especially after donning the VR headset on top.

A Handheld Stylus for Enhanced Dynamic Interactions

Using a whiteboard marker as inspiration, we designed a housing for Chasm in a stylus formfactor. The front half of the housing houses Chasm's components while the other half is solid plastic sized to be similar to a whiteboard marker. Users hold the marker in the grip position shown in Figure 1 with their thumb resting on the end effector. The thumb would then experience shear force from the actuator creating the illusion of impact, stiffness, force, weight or texture. The body of the marker prototype was 3D printed from ABS plastic. To track the position of the marker to be rendered in VR, the user worn an Oculus Touch controller with a Velcro strap securing it around their palm, as shown in Figure 1.

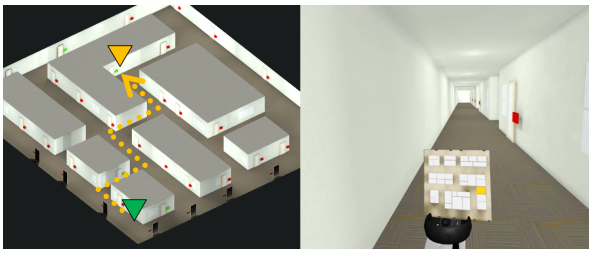

Figure 11. (left) An overview of the maze (right) The view from the VR headset while the participant views the map

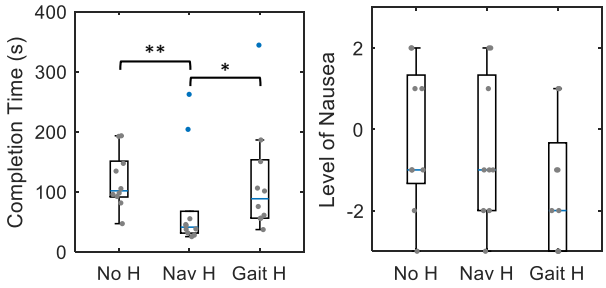

Figure 12. Box plots for completion time (left) and induced nausea level (right) while navigating in the VR maze.

Simulation Model

We used a "god object" model [39] to render haptic feedback on the thumb while the user interacted with objects using a virtual tool. The virtual tip of the marker, as seen by the user, cannot penetrate objects. When the actual position of the tip penetrates the virtual object, a force corresponding to the difference between the displacements of the virtual marker and the actual marker was rendered as skin stretch on the thumb. Figure 13 shows a simple implementation of a button press. When the tip of the real marker initiated the contact with the virtual button, the displacement of the button (d_B) and the displacement between the button and the tip (d_P) are both zero. As the tip pressed in the button, the resulting movement of the button in the visual scene is a function of the actual tip displacement. The ratio of the tip displacement (control, $C = d_B + d_P$) to the button displacement (display, $D = d_B$) induces the "pseudo-haptic" stiffness of the button, without any haptic cue [23,32]. The movement of the virtual button was governed by its stiffness (k_B), and the resulting force feedback was rendered as $F_P = k_P \times d_P$. The pseudo-haptic ratio is:

$$C/D = \frac{d_P + d_B}{d_B} = 1 + \frac{k_B}{k_P} \qquad (1)$$

The value of k_P was assigned to 2500 (N_v/m, where N_v is the Newton in game engine units) to compensate with the scaling in the Unity Engine and to render k_B up to 10000 (N_v/m) by displacing to the extreme position of Chasm's moving carriage, i.e., a maximum skin-stretch of 3.42 mm. The carriage displacement (d_C) is linearly scaled to d_P and renders instantaneous forces (F_P) on the thumb.

Psychophysical Study

In order to assess the usability of stretch cues on fingers for dynamic manual task, we ran a psychophysical study to evaluate the effectiveness of Chasm to render stiffness of a button press in the virtual environment. Thirteen participants (9 males, ages ranging from 25 to 44, median age: 28 years old, all righthanded) took part in the study. Participants were asked to sit on a chair, with the righthand controller strapped to the right hand holding the marker prototype and donned an Oculus Quest headset.

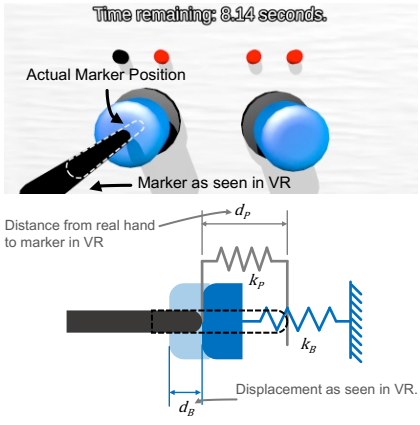

Figure 13. A simulation model for button pressing in VR

In each trial, participants were asked to use the marker to press into two buttons placed side by side and identify the button with larger stiffness. A reference stiffness of 5000 N_v/m was randomly assigned to one button and the other button (target) was assigned the stiffness from one of 12 values with higher or lower stiffness between 1000 - 9000 N_v /m. Participants were told that they could feel each button twice and enter their response within the 10-second-long trial. Each target stiffness was repeated four times with the total of 48 trials per test condition.

Three conditions were tested per participant: In the visual only (V) condition, pseudo-haptic feedback was presented with k_P set to 2500 N_v/m. In the haptic only (H) condition, participants felt skin stretch cues of reference and target stiffnesses through the marker displacement d_C, and k_P was set to infinity to obtain the C/D ratio of 1 for both button presses. In the visual-haptic (VH) conditions, both pseudo-haptic and congruent skin stretch cues were presented simultaneously. The levels and ranges of skin stretch and pseudo-haptic stiffnesses were determined in a pilot, where the extreme levels of stiffness were discerned ~10% and ~90% of times from the reference stiffness. Participants completed all three conditions presented in a random order, therefore completing 144 trials which lasted roughly 30 minutes including breaks. Throughout the experiment, participants wore headphones playing pink noise.

The experimental responses were combined for all participants and proportion of "yes" responses that the button is stiffer were plotted against the target stiffness (Figure 14). Psychometric curves are fitted to the means and the error bars represent standard error of the means. A two way repeated measure ANOVA indicated significant effect of stiffness

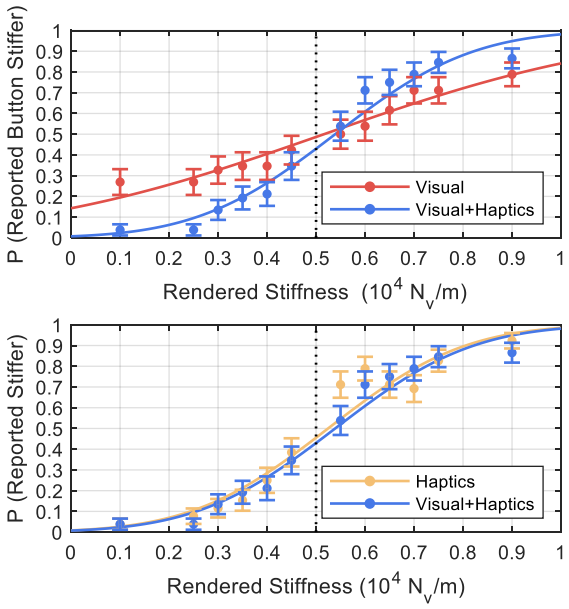

Figure 14. Psychometric plots comparing: (top) the V and VH conditions for the stiffness perception experiment and (bottom) the H and VH conditions

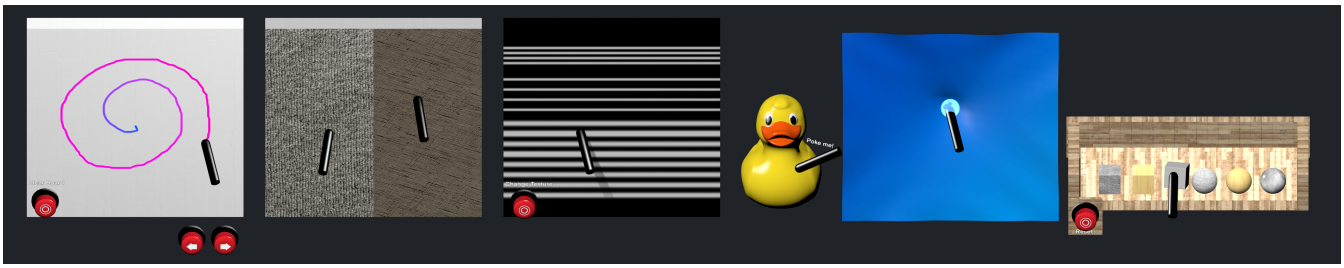

Figure 15. Demonstration boards for the for the marker prototype.

[$F(11,110)=10.9$; $p<0.001$] and test condition [$F(2,20)=6.6$; $p<0.01$] on the probability of yes response, while stiffness-condition interaction term was not significant ($p=0.55$). The slope of VH is much steeper than that of V, indicating better stiffness discriminability with the inclusion of haptic cues (Weber Fraction in V: 0.63 and VH: 0.297). In fact, improvement in sensitivity was entirely due to haptic cues (WF in H: 0.297) indicating effectiveness of skin-stretch in dynamical manual tasks.

Interactive Scenarios

To evaluate the real-world use of Chasm's stylus prototype, we generated a set of scenarios in a VR experience presented as a series of "boards" the user can scroll through using two buttons (Figure 15). The user dons an Oculus Quest headset and holds the marker as shown in Figure 1. In all scenarios, the marker is represented as a black cylinder with a rounded tip. The marker cannot penetrate most objects presented and is tied to a virtual spring to the actual marker location, creating a pseudo-haptic weight or force illusion upon contact similar to the technique used in the psychophysical study (Equation 1).

Whiteboard. A virtual whiteboard is presented as a 1 × 1 meter square with a lightly textured surface. The user uses the virtual marker to draw on the surface of the whiteboard. Chasm renders a small "bump" upon contact with the board, simulating a constant pressure from touching the board. If the user starts to move the marker on the surface, a line is visually generated along with a vibration of 75 Hz. Once the user removes the marker from the board, another "bump" is rendered, simulating the release of pressure from the board.

Textures. Two different textures are presented side by side, one resembles a rough texture and the other resembles a smoother texture. Both textures have the same behavior as the whiteboard. The rough texture has a 25 Hz vibration cue while the smoother texture has a 40 Hz vibration cue.

Texture to Displacement Map. This experience serves a demonstration to encode visual textures (like colors or grey shades) to haptic cues. The marker's tip samples the texture in contact with it and commands Chasm's displacement corresponding to the sampled intensity in the red channel. Thus, the haptic texture can be authored using images, drawings and pictures. Alternatively, the user could see one texture being displayed and feel another invisible texture using a separate channel for enhanced haptic cues.

3D Model. A textured, large, 3D rubber ducky is rendered in the scene. The user pokes the duck with the marker in order to create the presence of a physical object being in the scene. Chasm renders a displacement when the actual marker penetrates the duck, but the marker does not penetrate visually in order to create a force effect. The user moves across the model to feel curves and ridges of the 3D model.

Cloth Simulation. The user is presented with an orb that attaches to the marker when the marker is in proximity with the cloth. Once the orb attaches, Chasm renders a subtle haptic impact. As the cloth is stretched in, Chasm renders shear force accordingly. At the end of the cloth's stretch, the user penetrates through the cloth and a "snap" haptic effect is played. This experience demonstrates the use of arbitrary haptic waveforms that were authored as presets beforehand.

Cubes and Spheres. The user is presented with a shelf of 3 cubic blocks and 3 spherical balls of approximately 15 × 15 × 15 cm in size. Each object has a unique mass that reacts to the user prodding them with the marker according to Unity's physics engine. The user experiences both pseudo-haptic weight and the sensation of force from Chasm's displacement according to how far the virtual marker is to the actual marker.

CONCLUDING REMARKS

We present *Chasm*, a compact, lightweight and scalable screw based haptic actuator that can render dynamic haptic feedback in a variety of applications. Advantageous features of the actuator are its broadband range, linear operating features and low power consumption. Chasm renders multidimensional haptic feedback by directly converting the fast motor speed to the motion of the end effector, thereby simultaneously stimulating the skin with low-frequency skin deformations and high-frequency vibrations. In a series of studies and embodiments, we show that Chasm is used to stimulate forces, texture, vibrations in dynamical manual tasks, and induce navigational cues and illusory locomotion cues. In our future work, we will extend our preliminary findings of inducing forces and locomotion with Chasm and determine its capacity in other embodiments of wearable skin deformation devices to enhance user experience in high sensory environments.

ACKNOWLEDGEMENTS

We would like to thank our collaborators and Facebook, Inc. for supporting the work.

REFERENCES

[1] Petteri Aimonen. Nanopb - protocol buffers with small code size. Retrieved September 1, 2019 from https://jpa.kapsi.fi/nanopb/

[2] Hrvoje Benko, Christian Holz, Michael Sinclair, and Eyal Ofek. 2016. NormalTouch and TextureTouch: High-fidelity 3D Haptic Shape Rendering on Handheld Virtual Reality Controllers. 717–728. DOI:https://doi.org/10.1145/2984511.2984526

[3] Stanley J. Bolanowski Jr, George A. Gescheider, Ronald T. Verrillo, and Christin M. Checkosky. 1988. Four Channels Mediate the Mechanical Aspects of Touch. *The Journal of the Acoustical Society of America* 84, 5: 1680–1694. DOI:https://doi.org/10.1121/1.397184

[4] Inrak Choi, Heather Culbertson, Mark R. Miller, Alex Olwal, and Sean Follmer. 2017. Grabity: A Wearable Haptic Interface for Simulating Weight and Grasping in Virtual Reality. In *Proceedings of the 30th Annual ACM Symposium on User Interface Software and Technology* (UIST '17), 119–130. DOI:https://doi.org/10.1145/3126594.3126599

[5] Seungmoon Choi and Katherine J. Kuchenbecker. 2013. Vibrotactile Display: Perception, Technology, and Applications. *Proceedings of the IEEE* 101, 9: 2093–2104. DOI:https://doi.org/10.1109/JPROC.2012.2221071

[6] Francesco Clemente and Christian Cipriani. 2014. A Novel Device for Multi-Modal Sensory Feedback in Hand Prosthetics: Design and Preliminary Prototype. In *2014 IEEE Haptics Symposium (HAPTICS)*, 569–573. DOI:https://doi.org/10.1109/HAPTICS.2014.6775518

[7] Nathan Dunkelberger, Jenny Sullivan, Joshua Bradley, Nickolas P Walling, Indu Manickam, Gautam Dasarathy, Ali Israr, Frances W. Y. Lau, Keith Klumb, Brian Knott, Freddy Abnousi, Richard Baraniuk, and Marcia K O'Malley. 2018. Conveying Language Through Haptics: A Multi-sensory Approach. In *Proceedings of the 2018 ACM International Symposium on Wearable Computers* (ISWC '18), 25–32. DOI:https://doi.org/10.1145/3267242.3267244

[8] Adrien Girard, Maud Marchal, Florian Gosselin, Anthony Chabrier, François Louveau, and Anatole Lécuyer. 2016. HapTip: Displaying Haptic Shear Forces at the Fingertips for Multi-Finger Interaction in Virtual Environments. *Frontiers in Robotics and AI*. DOI:https://doi.org/10.3389/fict.2016.00006

[9] Brian Gleeson, Scott Horschel, and William Provancher. 2011. Design of a Fingertip-Mounted Tactile Display with Tangential Skin Displacement Feedback. *Haptics, IEEE Transactions on* 3: 297–301. DOI:https://doi.org/10.1109/TOH.2010.8

[10] Sidhant Gupta, Tim Campbell, Jeffrey R. Hightower, and Shwetak N. Patel. 2010. SqueezeBlock: Using Virtual Springs in Mobile Devices for Eyes-free Interaction. In *Proceedings of the 23Nd Annual ACM Symposium on User Interface Software and Technology* (UIST '10), 101–104. DOI:https://doi.org/10.1145/1866029.1866046

[11] Alexandra Ion, Edward Jay Wang, and Patrick Baudisch. 2015. Skin Drag Displays: Dragging a Physical Tactor Across the User's Skin Produces a Stronger Tactile Stimulus Than Vibrotactile. In *Proceedings of the 33rd Annual ACM Conference on Human Factors in Computing Systems* (CHI '15), 2501–2504. DOI:https://doi.org/10.1145/2702123.2702459

[12] Ali Israr, Siyan Zhao, and Oliver Schneider. 2015. Exploring Embedded Haptics for Social Networking and Interactions. 1899–1904. DOI:https://doi.org/10.1145/2702613.2732814

[13] Kenneth O. Johnson. 2001. The Roles and Functions of Cutaneous Mechanoreceptors. *Current Opinion in Neurobiology* 11, 4: 455–461. DOI:https://doi.org/10.1016/s0959-4388(00)00234-8

[14] Lawrence H. Kim, Pablo Castillo, Sean Follmer, and Ali Israr. 2019. VPS Tactile Display: Tactile Information Transfer of Vibration, Pressure, and Shear. *Proc. ACM Interact. Mob. Wearable Ubiquitous Technol.* 3, 2: 51:1–51:17. DOI:https://doi.org/10.1145/3328922

[15] Anatole Lecuyer, Sabine Coquillart, Abderrahmane Kheddar, Paul Richard, and Philippe Coiffet. 2000. Pseudo-Haptic Feedback: Can Isometric Input Devices Simulate Force Feedback? 83. DOI:https://doi.org/10.1109/VR.2000.840369

[16] Jack M. Loomis and Susan J. Lederman. 1986. Tactual perception. In *Handbook of perception and human performance, Vol. 2: Cognitive processes and performance*. John Wiley & Sons, Oxford, England, 1–41.

[17] Jens Maiero, David Eibich, Ernst Kruijff, Andre Hinkenjann, Wolfgang Stuerzlinger, Hrvoje Benko, and Gheorghita Ghinea. 2019. Back-of-Device Force Feedback Improves Touchscreen Interaction for Mobile Devices. *IEEE transactions on haptics* 12, 4: 483–496. DOI:https://doi.org/10.1109/TOH.2019.2911519

[18] D. Ian McCloskey. 1988. Kinesthesia, Kinesthetic Perception. In *Sensory Systems: II: Senses Other than Vision*, Jeremy M. Wolfe (ed.). Birkhäuser, Boston, MA, 36–38. DOI:https://doi.org/10.1007/978-1-4684-6760-4_17

[19] Kouta Minamizawa, Souichiro Fukamachi, Hiroyuki Kajimoto, Naoki Kawakami, and Susumu Tachi. 2007. Gravity Grabber: Wearable Haptic Display to Present Virtual Mass Sensation. In *ACM SIGGRAPH 2007 Emerging Technologies* (SIGGRAPH '07). DOI:https://doi.org/10.1145/1278280.1278289

[20] Kouta Minamizawa, Domenico Prattichizzo, and Susumu Tachi. 2010. Simplified Design of Haptic Display by Extending One-Point Kinesthetic Feedback to Multipoint Tactile Feedback. In *2010 IEEE Haptics Symposium*, 257–260.

DOI:https://doi.org/10.1109/HAPTIC.2010.5444646
[21] Stefano Mintchev, Marco Salerno, Alexandre Cherpillod, Simone Scaduto, and Jamie Paik. 2019. A Portable Three-Degrees-of-Freedom Force Feedback Origami Robot for Human–Robot Interactions. *Nature Machine Intelligence* 1, 12: 584–593. DOI:https://doi.org/10.1038/s42256-019-0125-1
[22] Claudio Pacchierotti, Gionata Salvietti, Irfan Hussain, Leonardo Meli, and Domenico Prattichizzo. 2016. The hRing: A Wearable Haptic Device to Avoid Occlusions in Hand Tracking. In *2016 IEEE Haptics Symposium (HAPTICS)*, 134–139. DOI:https://doi.org/10.1109/HAPTICS.2016.7463167
[23] Evan Pezent, Ali Israr, Majed Samad, Shea Robinson, Priyanshu Agarwal, Hrvoje Benko, and Nick Colonnese. 2019. Tasbi: Multisensory Squeeze and Vibrotactile Wrist Haptics for Augmented and Virtual Reality. In *2019 IEEE World Haptics Conference (WHC)*, 1–6. DOI:https://doi.org/10.1109/WHC.2019.8816098
[24] Sirawat Pitaksarit. 2019. *5argon/protobuf-unity*. Retrieved December 24, 2019 from https://github.com/5argon/protobuf-unity
[25] Christopher J. Ploch, Jung Hwa Bae, Wendy Ju, and Mark Cutkosky. 2016. Haptic Skin Stretch on A Steering Wheel for Displaying Preview Information in Autonomous Cars. In *2016 IEEE/RSJ International Conference on Intelligent Robots and Systems (IROS)*, 60–65. DOI:https://doi.org/10.1109/IROS.2016.7759035
[26] Ivan Poupyrev and Shigeaki Maruyama. 2003. Tactile Interfaces for Small Touch Screens. In *Proceedings of the 16th Annual ACM Symposium on User Interface Software and Technology* (UIST '03), 217–220. DOI:https://doi.org/10.1145/964696.964721
[27] Domenico Prattichizzo, Francesco Chinello, Claudio Pacchierotti, and Monica Malvezzi. 2013. Towards Wearability in Fingertip Haptics: A 3-DoF Wearable Device for Cutaneous Force Feedback. *Haptics, IEEE Transactions on* 6: 506–516. DOI:https://doi.org/10.1109/TOH.2013.53
[28] Nicolaas Prins and Frederick A. A. Kingdom. 2018. Applying the Model-Comparison Approach to Test Specific Research Hypotheses in Psychophysical Research Using the Palamedes Toolbox. *Frontiers in Psychology* 9. DOI:https://doi.org/10.3389/fpsyg.2018.01250
[29] William R. Provancher, Mark R. Cutkosky, Katherine J. Kuchenbecker, and Günter Niemeyer. 2005. Contact Location Display for Haptic Perception of Curvature and Object Motion. *International Journal of Robotics Research* 24, 9: 691–702. DOI:https://doi.org/10.1177/0278364905057121
[30] William R. Provancher and Nicholas D. Sylvester. 2009. Fingerpad Skin Stretch Increases the Perception of Virtual Friction. *IEEE Transactions on Haptics* 2, 4: 212–223. DOI:https://doi.org/10.1109/TOH.2009.34
[31] Zhan Fan Quek, Samuel B. Schorr, Ilana Nisky, William R. Provancher, and Allison M. Okamura. 2015. Sensory Substitution and Augmentation Using 3-Degree-of-Freedom Skin Deformation Feedback. *IEEE Transactions on Haptics* 8, 2: 209–221. DOI:https://doi.org/10.1109/TOH.2015.2398448
[32] Majed Samad, Elia Gatti, Anne Hermes, Hrvoje Benko, and Cesare Parise. 2019. Pseudo-Haptic Weight: Changing the Perceived Weight of Virtual Objects By Manipulating Control-Display Ratio. In *Proceedings of the 2019 CHI Conference on Human Factors in Computing Systems* (CHI '19), 320:1–320:13. DOI:https://doi.org/10.1145/3290605.3300550
[33] Samuel B. Schorr and Allison M. Okamura. 2017. Fingertip Tactile Devices for Virtual Object Manipulation and Exploration. In *Proceedings of the 2017 CHI Conference on Human Factors in Computing Systems* (CHI '17), 3115–3119. DOI:https://doi.org/10.1145/3025453.3025744
[34] Pratheev Sreetharan, Ali Israr, and Priyanshu Agarwal. 2019. A Compact Skin-Shear Device using a Lead-Screw Mechanism. In *2019 IEEE World Haptics Conference (WHC)*, 527–532. DOI:https://doi.org/10.1109/WHC.2019.8816105
[35] Lei Tian, Aiguo Song, and Dapeng Chen. 2016. A Novel Haptic Stylus for Mobile Terminal. In *Haptics: Perception, Devices, Control, and Applications* (Lecture Notes in Computer Science), 338–349. DOI:https://doi.org/10.1007/978-3-319-42321-0_31
[36] N. G. Tsagarakis, T. Horne, and D. G. Caldwell. 2005. SLIP AESTHEASIS: A Portable 2D Slip/Skin Stretch Display for the Fingertip. In *Proceedings of the First Joint Eurohaptics Conference and Symposium on Haptic Interfaces for Virtual Environment and Teleoperator Systems* (WHC '05), 214–219. DOI:https://doi.org/10.1109/WHC.2005.117
[37] Robert J. Webster III, Todd E. Murphy, Lawton N. Verner, and Allison M. Okamura. 2005. A Novel Two-dimensional Tactile Slip Display: Design, Kinematics and Perceptual Experiments. *ACM Trans. Appl. Percept.* 2, 2: 150–165. DOI:https://doi.org/10.1145/1060581.1060588
[38] Huichan Zhao, Aftab M. Hussain, Mihai Duduta, Daniel M. Vogt, Robert J. Wood, and David R. Clarke. 2018. Compact Dielectric Elastomer Linear Actuators. *Advanced Functional Materials* 28, 42: 1804328. DOI:https://doi.org/10.1002/adfm.201804328
[39] Craig B. Zilles and J.K. Salisbury. 1995. A Constraint-Based God-Object Method for Haptic Display. In *Proceedings 1995 IEEE/RSJ International Conference on Intelligent Robots and Systems. Human Robot Interaction and Cooperative Robots*, 146–151 vol.3. DOI:https://doi.org/10.1109/IROS.1995.525876
[40] FAULHABER SR 1016 ... SR. Retrieved September 1, 2019 from https://www.faulhaber.com/en/products/series/

[41] Kerk 5/64" (2mm) Lead Screw. Retrieved December 24, 2019 from https://www.haydonkerkpittman.com/products/lead-screws-and-nuts/lead-screws-by-size/5-64-2mm
[42] AS5311 - High Resolution Linear Position Sensor – Hall IC - ams | ams. Retrieved September 1, 2019 from https://ams.com/as5311
[43] DRV8835 1.5A low voltage stepper or single/dual brushed DC motor driver w/ dual supplies (PWM or PH/EN ctrl) | TI.com. Retrieved September 1, 2019 from http://www.ti.com/product/DRV8835
[44] Protocol Buffers. *Google Developers*. Retrieved September 1, 2019 from https://developers.google.com/protocol-buffers